Evaluation of Massive EGR and Miller Cycle Strategies for Mixing-Controlled Low Temperature Combustion in a HD Diesel Engine

Jesús Benajes, Santiago Molina, Ricardo Novella*, Eduardo Belarte
CMT-Motores Térmicos
*Universitat Politècnic*a de *Valènci*a
*Camin*o d*e Ver*a *s/n*, *46022*, *Valenci*a *(Spain*)
Tel. *(0034*) *96 387 76 50* / *Fa*x *(0034*) *96 387 76 59*

Abstract

The future of compression ignition engines depends on their ability for keeping their competitiveness in terms of fuel consumption compared to spark-ignition engines. In this competitive framework, the Low Temperature Combustion (LTC) concept is a promising alternative to decrease NOx and soot emissions. Thus, this research focuses on implementing the LTC concept, but keeping the conventional mixing-controlled combustion process to overcome the well-known drawbacks of the highly-premixed combustion concepts, including load limitations and lack of combustion control.

Two strategies for implementing the mixing-controlled LTC concept were evaluated. The first strategy relies on decreasing the intake oxygen concentration introducing high rates of cooled EGR. The second strategy consists of decreasing the compression temperature by advancing the intake valves closing angle to reduce the effective compression ratio, compensating the air mass losses by increasing boost pressure (Miller cycle). These strategies were tested in a single-cylinder heavy-duty research engine. Additionally, 3D-CFD modeling was used to give insight into local in-cylinder conditions during the injection-combustion process.

Results confirm the suitability of both strategies for reducing NOx and soot emissions, while their main drawback is the increment in fuel consumption. However, they present intrinsic differences in terms of local equivalence ratios and temperatures along combustion.

Keywords:

Compression ignition engines; Emissions control; Engine efficiency; Low temperature combustion; Miller cycle

* *Corresponding author*
Email: rinoro@mot.upv.es
Phone: (0034) 96 387 76 50 (Ext: 76544) // Fax: (0034) 96 387 76 59

1. Introduction

The major use of Diesel engines is heavy duty applications, because of their high fuel efficiency, durability, reliability and their high torque output. However, the gas exhausted by diesel engines contains undesirable and harmful species, which have to be reduced according with the newest emissions regulations. On this concern, the scientific community, in close collaboration with the engine manufacturers, is focusing their efforts in a combination of in-cylinder reduction strategies and exhaust gas after-treatment technologies. Due to the difficulties faced for reducing the cost of after-treatment devices, in-cylinder emission control strategies are still attractive to reduce simultaneously soot and NOx engine-out emissions.

Highly premixed combustion concepts have been widely investigated as combustion technologies to avoid soot and NOx engine-out emissions [1]. These strategies use volumetric auto-ignition and combustion in lean or dilute mixtures for which combustion temperatures are too low for significant NOx formation, and air-fuel mixtures (A/F) are too lean for soot formation. To achieve the high degree of fuel-air mixing needed for premixed combustion, researchers have found that the fuel injection event must be concluded prior to auto-ignition [2], [3]. Successful results have been obtained by means of highly premixed combustion strategies [4], [5]. However, despite the recent research efforts on this combustion concept, ignition timing control and load limit still remain as the main challenge for its practical application; an increase on the local equivalence ratios results in a fast transition to knocking combustion [6].

Conventional mixing-controlled Diesel combustion is well known for its suitability at complete engine operation range. Nevertheless, this combustion strategy relies on exhaust gas after-treatment technologies for controlling NOx and/or soot emissions. Through detailed studies, many researchers confirmed how high temperatures at the stoichiometric diffusion flame surface imply high NOx formation [7 - 9]; and also that soot formation occurs inside the envelope of the diffusion flame, in the high temperature and fuel-rich regions of the spray after the lift-off length [10 - 13]. Soot is finally exhausted if it is not further oxidized in later phases of the combustion process.

On light of the drawbacks from those combustion strategies, mixing-controlled low temperature combustion (MC-LTC) strategy arises as an alternative to overcome the lack of ignition timing control of the highly premixed strategies as well as the NOx-soot

trade-off characteristic of the conventional diffusive combustion. Pickett et al. [14] reported three different alternatives to attain mixing-controlled non-sooting low flame temperature diesel combustion in an optically-accessible, quiescent constant-volume combustion vessel. The first one is based on the use of reduced nozzle hole diameters; the second consists of sharply decrease the ambient gas temperature; and the third needs the use of extensive exhaust gas recirculation (EGR) to reduce the ambient gas oxygen concentration (YO_2). Different investigations confirmed the feasibility of the mixing-controlled low temperature combustion for avoiding NOx and soot emissions formation in a HSDI engine [15], [16]. There, the MC-LTC strategy was implemented by introducing massive EGR rates, so following the third alternative. Authors stated that the sootless and zero-NOx combustion process intrinsically generates high levels of HC and CO emissions, lowering engine efficiency.

With the aim of overcoming the drawbacks from using extensive EGR, Benajes et al. [17] investigated the suitability of the Atkinson cycle for lowering the in-cylinder gas temperature. It was performed by advancing the intake valves closing angle, keeping constant intake and exhaust pressures, in a HD diesel engine equipped with a fully variable valve actuation (VVA) system. Results corroborated the potential from Atkinson cycle for reducing the in-cylinder gas temperature during the compression stroke, but also the gas pressure and its density. According with the results obtained by Jia et al. [18], NOx emissions decrease due to the lower temperatures along the combustion process, but the spray mixing process is intrinsically slowed down as a result of the lower gas density. Therefore, the mixing-controlled combustion process deteriorates and soot, CO and fuel consumption increase.

In this framework, the following investigation focuses on improving the existing knowledge on the MC-LTC concept, and also on comparing the two key strategies available for implementing this advanced combustion concept, the massive EGR and the Miller cycle. In this case the massive EGR strategy was implemented as usual, while the Miller cycle was implemented by increasing the boost pressure. The objective was to recover the air mass loss due to the shortened intake event, avoiding the well-known drawbacks of the Atkinson cycle as a result of the lack of air for sustaining a suitable combustion process. Thus, this investigation was carried out with the aim of understanding the benefits/drawbacks provided by these two strategies.

The study includes a sequential analysis of the combustion process, final exhaust emissions and fuel consumption trends by combining direct experimental data with the detailed information on the local in-cylinder conditions obtained from 3D-CFD simulations. This information was combined for comparing the two strategies not only in terms of the final engine out emissions and efficiency, but also considering the detailed mechanisms involved in NOx and soot emissions control by analyzing the local conditions along the combustion process.

2. Objectives and methodology

This research work was focused on achieving non-sooting and low flame temperature mixing-controlled combustion in a HD Diesel engine by means of two different strategies to conclude which are their benefits and drawbacks. The massive EGR strategy relies on decreasing the intake oxygen concentration by means of introducing high rates of cooled external EGR. The Miller cycle strategy consists of decreasing the compression temperature by reducing the engine effective compression ratio (CR_{ef}) while increasing boost pressure to compensate the air mass loss. Firstly, these two strategies were analyzed in detail to identify the mechanisms for attaining non-sooting and low flame temperature mixing-controlled combustion. The analysis was carried out by combining direct engine testing with 3D-CFD modeling to relate the trends followed by pollutant emissions with the in-cylinder local conditions. To conclude, both strategies were critically compared and their potential for further development was evaluated.

The methodology followed to analyze massive EGR and Miller cycle strategies was based on a set of parametrical studies varying the intake oxygen concentration and the effective compression ratio. This way to proceed enables the understanding of isolated effects and it is suitable for comparing the strategies. The basic engine operation conditions are defined by 1200 rpm engine speed keeping a constant injected fuel mass of 91.2 mg/cycle.

Both parametrical studies are shown in the A/F-EGR map included in Figure 1. There is shown how the massive EGR strategy was implemented by reducing the YO_2 at the beginning of combustion ($YO_{2,SOC}$) from 16% to 10%, but keeping constant the YO_2 at the end of combustion ($YO_{2,EOC}$). Since A/F = 19 was kept constant, the higher EGR the higher required boost pressure (BP). This procedure avoids the well-known negative

effects of reducing $YO_{2,EOC}$ over soot emissions [19]. Settings used to implement this strategy are listed in table 1. The Miller cycle was implemented to reduce the CR_{ef} from 14.4 to 8, shortening the intake stroke by advancing the intake valves closing angle (IVC). The reduction in air mass flow rate caused by this shortened intake stroke was compensated increasing boost pressure. A/F ratio and EGR ratio were kept constant for all points related to Miller cycle strategy, thus, these points overlap in the A/F–EGR map. Detailed settings used to implement this strategy are included in table 2.

The study has been performed to investigate the basis of MC-LTC concepts. Further development, using the knowledge obtained from this research, will be needed to extend the concept to the whole engine operation map.

3. Experimental setup

In comparison with multi-cylinder engines, single-cylinder engines generate more accurate data [3]. Accordingly, a single-cylinder engine was used in this research work. The main characteristics of the engine and the test cell are described in the following sub-sections.

3.1. Single cylinder engine

The engine is a single-cylinder, four-stroke, direct-injection Diesel research engine, representative of commercial truck engines. Basic specifications of this engine are detailed in Table 3.

The engine is equipped with flexible injection hardware. The main characteristic of this hardware is its capability to amplify common-rail fuel pressure by means of a hydraulic piston directly installed inside the injector.

In this study a 20 CAD length injection rate was performed each cycle in order to generate a mixing-controlled combustion process. As bibliography suggests, high injection pressure (2350 bar) and a small injector nozzle (100 μm) were used to promote lifted-flame combustion.

Additionally, the engine is equipped with a hydraulic VVA system, so all valves are independently actuated by different hydraulic pistons (one per valve), which are controlled by a specific electronic control unit. The main benefit of this VVA system is its extremely high flexibility, including variable timing, variable duration and variable lift for each intake and exhaust valve. If necessary, two intake and/or exhaust events per

cycle can also be carried out. Thus, using this system, many strategies can be performed in the engine. As a counterpart, this system requires an adapted cylinder head different from the conventional design (although the structural changes are not extreme) and also a dedicated oil circuit in addition to the standard oil lubricating system.

One of the specificities of the hydraulic valve actuation is a fast-motion intake and exhaust valve lift profiles. Increasing the exhaust valves opening and closing speeds is interesting for reducing gas energy losses by shortening the time in which the exhaust gas flow evolves under sonic conditions [20]. However, this fast-motion together with the very little clearance between the piston and valves when the piston is close to top dead centre (TDC), make the valve overlap at breathing TDC impossible due to direct mechanical interference between the piston and the valves. This lack of valve overlap slightly reduces the engine volumetric efficiency.

3.2. Test cell

The engine was installed in a fully instrumented test cell, with all the auxiliary facilities required for its operation and control, as Figure 2 shows.

To achieve stable intake air conditions, an externally driven screw compressor supplied the required boost pressure before passing through an air dryer. Intake air pressure was adjusted in the intake settling chamber, while intake temperature was controlled in the intake manifold after mixing with EGR. The exhaust backpressure produced by the turbine in a real engine was replicated by means of a valve placed in the exhaust system, controlling the pressure in the exhaust settling chamber.

Due to the benefits in terms of emissions formation control from cooling EGR [21], a highly cooled EGR system was installed on the engine test bench, Exhaust gas was extracted from the exhaust settling chamber and forced to flow across a first heat exchanger to decrease its temperature. Water condensed in this first heat exchanger was separated from the gas stream by means of a centrifugal filter and the resulting dried gases flowed across an additional filter to remove solid particles. Then, an externally driven roots-type supercharger was used to increase the exhaust gas pressure over the intake pressure. This compression increased the exhaust gas temperature; hence, the exhaust gas was also forced to flow across a second heat exchanger before getting in a dedicated EGR settling chamber equipped with an electrical heater. Finally, the exact EGR rate was controlled by a valve placed between the EGR settling chamber and the

intake pipe. The temperature regulation was performed upon the EGR-fresh air mixture by means of a temperature sensor in the intake manifold.

The EGR rate was calculated using the experimental measurement of intake and exhaust CO_2 concentration. The concentrations of NO_X, CO, HC, intake and exhaust CO_2, and O_2 were measured with specific state-of-the-art analyzers. Smoke emission was measured with a variable sampling smoke meter, providing results directly in Filter Smoke Number units (FSN) that were transformed into dry soot mass emissions by means of the correlation proposed by Christian et al. [22]. The fuel injection rate was measured in a commercial test rig following the Bosch system [23].

The in-cylinder pressure traces from a piezo-electric transducer were recorded during 100 engine cycles in order to compensate for dispersion in engine operation. The recorded values of in-cylinder pressure were processed by means of a combustion diagnosis code CALMEC [24, 25].

The rate of heat release (RoHR) and all the key related combustion parameters were provided by the combustion diagnosis code, while the adiabatic flame temperature (T_{ad}) and the spray mixing capacity were estimated from the experimental results according to the procedures and hypotheses detailed by Benajes et al. [19].

To ensure the reliability of the provided results, every operation point was measured three times and a reference point was controlled before every testing session to assure tests repeatability along the study. Additionally, Table 4 contains the accuracy of the different experimental devices (sensors, analyzers…) used in this research work. This data has been obtained following rigorously the calibration procedures recommended by their respective manufacturers. After a detailed check of the accuracy levels, they are fully comparable with those usually observed in similar investigations in the frame of internal combustion engines [26], so the expected errors on final results are considered in the state-of-the-art and then suitable for performing the studies.

4. Computational model

3D-CFD calculations were performed by means of StarCD CFD code [27]. The ES-ice preprocessing software from CD-Adapco was used for mesh generation and motion. Due to the equally spaced 8-hole nozzle, the computational domain comprises a 45 degree sector of the combustion chamber, with periodic boundary conditions. Figure 3 shows the final mesh configuration where an additional volume at the crevice region is

employed in order to match engine compression ratio. In this research the adopted mesh for performing the CFD simulations is not oriented according to the spray geometry. However, the local values of the fluid velocity are interpolated on basis of hexahedral cells vertex-based values, and for any other non-hexahedral cell shape the gradients method is used. For any other carrier fluid property the gradients method is always used. Thus, the non-desirable effects associated to the non-oriented mesh following the spray path are at least partially avoided. Nevertheless, to be sure about the quality of the spray dynamics simulation, a particular study of mesh sensitivity was carried out until reaching suitable mesh convergence before running the simulations, and more refined meshes, with larger computational cost, reported very close results. Therefore, the mesh included in Figure 3 with a typical grid size of 0.75 mm inside the bowl was selected.

A standard lagrangian approach (DDM [28]) is used for fuel spray modeling. Huh-Gosman [29] and Reitz-Diwakar [30] models are applied for primary and secondary break-up. Fuel physical properties are given by the so-called DF1 [31] diesel fuel surrogate.

The combustion model selected for performing this investigation is the version of the ECFM-3Z integrated in the Star-CD platform [27], [32]. This model combines different sub-models for auto-ignition, premixed / diffusion flames and a sub-grid mixing model in order to account for turbulence-chemistry interaction. More in detail, the mixing sub-model stands for three zones of mixing in which the local mixture is decomposed into the unmixed fuel, the unmixed air plus EGR gas and the mixed gases. Then, the auto-ignition sub-model is based on the conditional unburned mixed gases and it predicts the auto-ignition delay using an Arrhenius-type correlation. Once auto-ignition is reached, the mixed fuel is burned at a rate determined by a chemical characteristic time and a flame kernel is created. Afterwards, the ECFM model is applied over the mixed gases to compute the premixed stage of combustion, where the flame surface density equation is solved. Then is calculated the diffusion part of the flame, where the Magnussen eddy break-up model is adopted and a kinetic reaction mechanism is introduced for CO and CO_2 mass fractions. A detailed description of this model can be found in the work of Colin and Benkenida [33].

Turbulent flow is modeled with the RNG k-ε model and, since this turbulence model is a high Reynolds number based model, it requires special treatment of the near-wall

region. Thus, standard wall functions were used to account for the interactions between the gas flow and the combustion chamber surfaces. These wall functions gave the cross stream profiles in terms of the normal distance y from the wall considering the y^+ value, which is the non-dimensional distance (based on local cell fluid velocity) from the wall to the first mesh node. In this case, the wall functions are expected to provide accurate results since the y^+ values are within 30 and 100. Additional details on these wall functions are available in the CFD code user manual [27].

As shown in Figure 3 the single layer of cells for the boundary layer has not been extended to the cylinder head on top mainly because of two different reasons. On one hand wall functions are sufficiently accurate for $y^+ < 100$. On the other hand, the topology of the mesh provides cells perpendicular to the cylinder head on top. Based on these two arguments, the use of a boundary layer on the top of the mesh, at the cylinder head, has been omitted since both conditions are fulfilled.

These wall boundary conditions were set assuming uniform wall velocity and uniform wall temperature (each phase sees a different heat flux and interphase heat transfer is possible) applied to all phases. The flow solver uses the PISO algorithm in order to solve pressure-velocity coupling. A second order scheme (MARS [27]) is used for momentum and turbulence equations, while first order upwind is applied for enthalpy and species equations.

Calculations run from IVC to EVO (exhaust valves opening), with 1e-5 s time-step during compression stroke and 1e-6 s from SoI to EVO. Both initial conditions at IVC and wall temperatures have been obtained from experimental data by means of in-house combustion diagnostic code CALMEC [24].

The data provided by the 3D-CFD code was validated against experimental data to assure the quality of the model. Figure 4 shows a suitable agreement between predictions from the computational model and experimental data in terms of cylinder pressure and also of RoHR profiles. Thus, after this verification the 3D-CFD model was used for complementing the analysis of the MC-LTC concepts in combination with the experimental results.

5. Results and discussion

The following section includes the analysis of the massive EGR and Miller cycle strategies, which were expected to attain ultra-low NOx and soot mixing-controlled low

temperature combustion. Firstly, for each strategy, instantaneous results of the combustion process are described, and afterwards, the analysis focuses on the results of specific engine-out emissions and fuel consumption. Then, the experimental results are related with in-cylinder local conditions from 3D-CFD modeling. Finally, both strategies are compared discussing their benefits in terms of pollutant emissions and fuel consumption.

5.1. Massive EGR Strategy

As was previously described, aside from using oxygenated fuels, the most extensively investigated option to implement the MC-LTC concept is the use of massive EGR. In this study $YO_{2,SOC}$ was reduced from 16% to 10% while A/F = 19 was kept constant. In order to reach these conditions, the rate of cooled EGR and the boost pressure were increased conveniently as is detailed in Table 1.

Experimental results in terms of instantaneous injection rate, RoHR, adiabatic flame temperature and mixing capacity, obtained sweeping the EGR rate, are shown in Figure 5 (left). Figure 5 (right) shows the evolution of the YO_2, gas density and spray mixing capacity as a function of the burned mass fraction (MBF) since this representation intrinsically enhances the relation between these parameters and the combustion process. This representation is interesting for comparing between different combustion strategies, because of its independence on the temporal coordinate.

Looking to the highest $YO_{2,SOC}$ trace of Figure 5, the RoHR has the structure of a conventional mixing-controlled combustion: a premixed combustion stage, where most fuel injected during the ignition delay is burnt; followed by a diffusive combustion stage, where the RoHR is controlled by the fuel-air mixing process; and the late diffusive combustion stage, that occurs after the end of injection (EoI). As the $YO_{2,SOC}$ decreases by increasing EGR, differences appear in the initial premixed and in the late mixing-controlled combustion stages. The first peak of premixed burn decreases due to the shortened ignition delay time and the worsening of the spray mixing capacity, caused by the lower $YO_{2,SOC}$. By contrast, along the late mixing-controlled combustion stage the instantaneous in-cylinder YO_2 converges, so the higher gas density results in similar spray mixing capacity. Furthermore, Figure 5 shows how from a given point, the spray mixing capacity is even higher, increasing the RoHR during this late mixing-controlled combustion stage.

Figure 6 shows the experimental trade-offs of averaged emissions and efficiency. This figure includes fuel indicated emission index (in g/kg_{fuel}) of soot, CO, HC and NOx, together with brake and indicated specific fuel consumption in relative. Additionally, 3D-CFD results have been used to gain insight of the experimental results. Figure 7 shows a ϕ-T map including the local equivalence ratio and temperature of each cell of the computational domain. For simplicity, only the results for 15%, 12% and 10% $YO_{2,SOC}$ have been plotted when 50% of the fuel is already burnt (at 3.8, 4.6 and 4.6 CAD aTDC, respectively). Behind those local conditions, this diagram includes the soot and nitrogen oxides (NO) formation regions mapped by Akihama et al. [34].

The INOx reduction observed increasing EGR (decreasing $Y_{O2,SOC}$) in Figure 6 is consistent with the lower adiabatic flame temperatures already shown in Figure 5. As expected, the lower temperatures in the flame during the combustion process slow down the thermal NO formation. Results from 3D-CFD calculations included in Figure 7 show how local conditions are shifted towards the low temperature region.

Regarding soot emissions, they are the result from a balance between formation and oxidation processes. Figure 5 (left) shows the transition to smoother RoHR as the $YO_{2,SOC}$ decreases from 16% to 12%, while Figure 5 (right) confirms a clear reduction in adiabatic flame temperatures during the late mixing-controlled combustion stage. This implies the worsening of the oxidation processes, explaining the increase of soot emissions shown in Figure 6. Results from 3D-CFD shown in Figure 7 confirm how the local conditions move in the direction of decreasing temperatures, but not enough to avoid the soot formation peninsula. Then, since the maximum local equivalence ratios in the reacting regions still high enough to form soot, for this $YO_{2,SOC}$ range, soot emissions are clearly controlled by the oxidation processes. The worsened oxidation processes explain the increment in soot emissions.

However, according to Figure 6 soot emissions are significantly reduced for $YO_{2,SOC}$ below 12%. Looking at Figure 7, local conditions are further displaced towards the low temperature region, avoiding the soot formation peninsula. Therefore, the combination of experimental results and CFD analysis corroborates how for this $YO_{2,SOC}$ range, soot emissions are controlled by avoiding formation processes.

Figure 6 illustrates how ICO slightly increases and IHC is almost constant in the zone where soot is controlled by the oxidation processes. By contrast, an important increase

of these emissions is observed in this figure when soot is controlled by formation processes. According to Figure 7, the important lowering of local temperatures leads to incomplete conversion of HC and CO into CO_2. This is a key drawback of this combustion strategy which affects negatively the combustion efficiency. This lower combustion efficiency and the extended combustion process agree with the large increase of ISFC and BSFC observed in Figure 6.

Comparing these results with those previously reported by Pickett and Siebers [14], despite the differences between a constant-volume combustion vessel and a single cylinder engine, in both cases the massive EGR strategy provided non-sooting combustion; avoiding soot inception by decreasing the maximum local temperatures. Moreover, comparing these results with those obtained in a HSDI Diesel engine [15], in both cases general trends observed reducing YO2,SOC are similar since sootless and zero-NOx combustion with sharply increased CO and HC and 5% higher ISFC was also observed.

5.2. Miller Cycle Strategy

In the previous section MC-LTC concept was implemented by introducing high rates of cooled EGR to reduce $YO_{2,SOC}$. As a main benefit, this combustion strategy was proven to be able to reduce simultaneously NOx and soot emissions. As a main drawback, it implies a strong penalty in terms of combustion efficiency and fuel consumption. In this section MC-LTC concept is implemented by using the Miller cycle to decrease the in-cylinder gas temperature, in an attempt to keep the emission benefits without the mentioned drawback. The effective compression ratio (CR_{ef}) was decreased from 14.4 to 8 by advancing the IVC, while A/F = 19 and $YO_{2,SOC}$ =15% were kept constant.

Despite of this extreme CR_{ef} reduction, the minimum in-cylinder gas mean temperature estimated by CALMEC combustion diagnosis code, just before the onset of combustion, was 777 K. The engine was operated with conventional diesel fuel with a cetane number close to 54, which auto-ignition temperature is around 750 K. Therefore, CR_{ef} was reduced without observing any ignition and stability problems, while the temperature after the compression stroke reaches values over this trigger temperature. This is supported by the coefficient of variation of the IMEP, which resulted to be around 1% in the worst case, without noticing any misfire during the experimental activities.

Following the same structure than Figure 5, the experimental results from the CR_{ef} sweep are shown in Figure 8. The starting point of the Miller cycle sweep has the structure of a conventional mixing-controlled combustion, as explained in the previous section. As CR_{ef} decreases by the Miller cycle effect the combustion process develops very differently compared to what was observed in Figure 5. Decreasing CR_{ef} implies the reduction of in-cylinder gas temperature and results in a longer ignition delay. In addition, the evolution of gas density and YO_2 along the combustion process is not affected since the intake pressure was increased and the intake air mass was conveniently recovered. Thus, the spray mixing capacity is not affected. This fact, added to the longer ignition delay, increases the fuel mass burnt during the premixed combustion stage, which is enlarged. Consequently, the diffusive combustion stage is progressively shortened, as RoHR traces in Figure 8 (left) show.

Equally structured than in Figure 6, Figure 9 contains the emissions and fuel consumption results from the Miller cycle sweep. Additionally, Figure 10 shows the ϕ-T map, including soot and NO formation regions, from the CFD calculations. For clarity, only the results for CR_{ef} 14.4, 11 and 8 have been plotted when 50% of the fuel is already burnt (at 3.8, 4 and 7.6 CAD aTDC, respectively).

As Figure 9 shows, the Miller cycle strategy decreases INOx emissions as the CR_{ef} is lowered. The maximum adiabatic flame temperatures shown in Figure 8 progressively decrease, but not as much as with the massive EGR strategy. The reduction in air mass flow rate caused by the shortened intake stroke was compensated increasing boost pressure. This higher boost pressure tends to increase combustion temperature, the opposite effect than the observed by reducing CR_{ef}. To analyze these effects, they have been quantified by normalizing them with respect to their values at the reference case of the Miller cycle study. Then, comparing the reference with the extreme Miller cycle cases BP increases from 1.65 up to 3.64 bar (120%), while the CR_{ef} decreases from 14.4 down to 8 (43%). Using as usual the maximum adiabatic flame temperature as an indicator of the combustion temperature, it decreases by around 4%. Consequently, the combustion temperature reduction caused by the lower CR_{ef} is greater than its increment associated to the higher boost pressure, and the final result of this opposite effects is the moderate decrement of the combustion temperature observed. Computational results in

Figure 10 confirm the slight local temperature decrease and the mixture movement away from the NO formation peninsula.

Figure 9 shows how Isoot emissions decrease with the CR_{ef} reduction. Longer ignition delays combined with constant spray mixing capacity result in more fuel mass burning in the premixed stage. Then, in the mixing-controlled combustion stage, the lowering of in-cylinder gas temperature increases the lift-off length and, since the spray mixing capacity is unaffected, the equivalence ratio at the lift-off decreases [12]. It is well known how soot precursors formation inside the reacting spray can be avoided by decreasing this equivalence ratio at lift-off [15], which justifies the observed reduction on Isoot. This behavior is clearly captured by the computational results included in Figure 10, where the local conditions shift towards the low equivalence ratio region, avoiding the soot formation peninsula.

As was previously described, the CR_{ef} reduction results in a slight reduction of mean gas and also flame temperatures during the combustion process. This trend implies a slight worsening of the oxidation processes, which agrees with the small increase of ICO and IHC emissions shown in Figure 9. This figure also shows a positive impact on ISFC from the shorter and more energetic combustion process observed when reducing CR_{ef}. However, BSFC results are worsened as it will be discussed in detail in the following section.

Comparing these results with those previously obtained by Benajes et al. [17], the benefits from using the Miller cycle instead of the Atkinson are evident since the mixing process is not worsened, and therefore, combustion does not get slower. As a result the simultaneous reduction of NOx and soot emissions is not followed by a sharp increment in CO emissions and additionally ISFC decreases.

5.3. Comparison of the two strategies for implementing MC-LTC concept

This comparison starts from common initial operating conditions: A/F = 19, $YO_{2,SOC}$ = 15% and CR_{ef} = 14.4. Then, both paths, reducing $YO_{2,SOC}$ and reducing CR_{ef} were followed as detailed in Tables 1 and 2.

Comparing the RoHR profiles between Figures 2 and 5, the ignition delay is slightly shortened for the massive EGR strategy while it increases with the Miller cycle strategy. In addition, decreasing $YO_{2,SOC}$ by adding EGR results in a worsened spray mixing capacity, but it keeps constant reducing CR_{ef} by implementing the Miller cycle. The

longer ignition delay and constant spray mixing capacity result in shorter and sharper combustion events for the Miller cycle strategy. Hence, the adiabatic flame temperatures are much more decreased using the massive EGR strategy than using the Miller cycle strategy.

Emissions and fuel consumption differences between both strategies can be analyzed comparing figures 6 and 9. As complementary information, to evaluate differences of local conditions between the strategies, Figure 11 is a ϕ-T map which compares the initial and the extreme operating conditions for both sweeps. This map was generated when 50% of the fuel is already burnt in all cases, and including the soot and NO formation regions.

Combustion differences observed comparing figures 2 and 5 agree with the engine emissions differences from figures 6 and 9 comparison. The higher impact of introducing massive EGR on adiabatic flame temperatures implies a sharper reduction of INOx emissions compared to that attained by using the Miller cycle strategy. Nevertheless, both combustion strategies provide very low INOx levels below 1 g/kg_{fuel}, which correspond to 0.2 g/kWh. These levels are well below the limit of 0.4 g/kWh imposed by EURO VI regulation.

Concerning Isoot emissions, increasing the EGR rate, initially they are controlled by formation processes; thus, they increase due to the worsening of the oxidation processes caused by the temperature reduction along the late mixing-controlled combustion stage. However, at a given point, Isoot emissions start to be controlled by soot formation processes; so, they decrease by avoiding the soot formation despite the deterioration of the oxidation processes. By contrast, using the Miller cycle, Isoot emissions get lowered despite the progressive in-cylinder temperature reduction and the consequent deterioration of the soot oxidation processes. In this case the balance between soot oxidation and formation processes is always dominated by avoiding the soot formation.

The differences in local conditions between both strategies shown in Figure 11 agree with the previously discussed emissions trends. The mixture distribution at the starting point conditions intersects the soot and NOx formation zones, but the local conditions evolution is very different between both strategies. Increasing EGR shifts the mixture distribution towards the low temperature region, avoiding NOx formation and soot formation regions despite the presence of richer equivalence ratios. Implementing the

Miller cycle shifts the mixture distribution towards the low equivalence ratio region, avoiding soot formation region and being on the limit of NOx formation because of the slight reduction of temperature at the stoichiometric equivalence ratio.

A key difference between these strategies consists in the important worsening of oxidation processes when ultra-low levels of Isoot and INOx emissions are simultaneously attained. To quantify this behavior, combustion efficiency has been calculated from experiments using Equation 1, and these results have been represented in Figure 12. Trends confirm how implementing the MC-LTC concept by massive EGR intrinsically worsens the combustion efficiency, due to the extreme reduction of the $YO_{2,SOC}$ required. Nevertheless, the Miller cycle strategy allows implementing the MC-LTC concept hardly affecting combustion efficiency.

$$\eta_{comb} = 1 - \frac{HC[\frac{mg}{s}]}{m_{fuel}\left[\frac{kg}{h}\right] \times \frac{10000}{36}} - \frac{CO[\frac{mg}{s}]}{4 \times m_{fuel}\left[\frac{kg}{h}\right] \times \frac{10000}{36}}$$

Equation 1: Combustion efficiency calculation.

The results obtained in terms of combustion efficiency agree with the ISFC results included figures 6 and 9. For the massive EGR strategy, ISFC increases as combustion efficiency is worsened and BSFC is controlled by ISFC. By contrast, when analyzing the Miller cycle strategy, combustion efficiency remains at around 99.5% while ISFC decreases and BSFC is not controlled by ISFC. Aside from other combustion parameters such as combustion phasing, heat transfer is expected to be the main reason explaining the ISFC trend. The lower in-cylinder temperatures generated by the Miller cycle decrease heat transfer through the combustion chamber walls. The comparison between figures 6 and 9 shows that using the Miller cycle strategy BSFC is worsened to almost the same level than the attained using the massive EGR strategy. Since for Miller cycle strategy BSFC is not controlled by ISFC, it is worth to investigate why BSFC increases. A study focused on the low pressure loop of the p-V diagram has been performed. Three points have been considered for this analysis, which are the initial operating condition and the extreme operating conditions for both strategies. Figure 13 shows the result from this study, where the positive and negative pumping work areas are marked with a plus and minus signs. The low pressure work has been quantified by means of CALMEC combustion diagnosis code and these values are included in the legend. Looking to the mentioned quantified areas, the lowest CR_{ef} test shows much

higher pumping work than the other two tests. The in-cylinder pressure during the exhaust stroke is always above pressure during the intake stroke, and that negative pumping work increases as the piston moves down after the IVC. In addition, the high levels of boost pressure required decrease the area of the high pressure loop by cutting its bottom side. Accordingly, the increase in terms of BSFC observed in Figure 9 is justified by the pumping work consumed by shortening the intake event to reduce the CR_{ef} and increasing the boost pressure to recover the air mass loss.

Previous analysis confirms how the increment of BSFC observed with the massive EGR strategy is directly associated to the intrinsic deterioration of the combustion process and ISFC, which cannot be avoided, so this is a strong limitation of this strategy. However, Miller cycle keeps the ISFC almost constant or even improves it since combustion develops properly, then this strategy is expected to be able to provide interesting levels in terms of BSFC, but the efforts to recover such levels should be shifted towards the development of turbocharging systems.

6. Conclusions

Present study focuses on investigating the potential of two different combustion strategies for the simultaneous reduction of NOx and soot emissions, in a HD single-cylinder research engine. The injection hardware and settings were adjusted to fit the MC-LTC concept requirements, so a small injection nozzle (100 μm) and high injection pressures (2350 bar) were used. Also multi-dimensional CFD simulations were performed to gain an insight of soot and NOx emissions formation, by means of ϕ-T maps, based on the predictions of in-cylinder local gas mixture conditions.

For implementing the first MC-LTC strategy, high rates of cooled EGR were added to the intake air mass with the aim of reducing the intake oxygen concentration without increasing the intake gas temperature. The following main conclusions were extracted from this study:

- Gas mixing capacity is initially worsened; the premixed stage of RoHR gets smoother and the adiabatic flame temperatures decreases.
- Local mixtures move towards the low temperature and medium-low equivalence ratio zone of the ϕ-T map, avoiding NOx and soot formation processes.

- The highly diluted conditions needed to decrease simultaneously NOx and soot emissions imply a strong reduction of combustion efficiency, increasing HC/CO emissions and fuel consumption.

Regarding the second MC-LTC strategy, Miller cycle was implemented by shortening the intake event duration, decreasing the effective compression ratio and keeping constant the intake air mass and $YO_{2,SOC}$. This study provided the next conclusions:

- No effect over the spray mixing capacity is observed. The in-cylinder gas temperature lowering increases the ignition delay and promotes the premixed combustion stage, resulting in sharper and shorter combustion profiles.
- NOx and soot emissions decrease by avoiding their corresponding formation processes (slightly lower temperatures and much leaner local equivalence ratios), while HC and CO emissions remain at low levels since their respective oxidation processes are not noticeably affected.
- The reduced heat transfer through the walls is expected to be the reason of the improvement of ISFC. However, the pumping work from the p-V low pressure loop gets much higher and this explains the BSFC worsening, which is the main drawback of this combustion strategy.

From this investigation, it is evident how the massive EGR strategy needs the worsening of the combustion process and ISFC to decrease NOx and soot emissions, while the Miller cycle strategy does not introduce any negative impact on this combustion process and ISFC. However, despite the important differences in terms of combustion development, both strategies result in an increase of BSFC. Finally, results confirm how both MC-LTC strategies are suitable for decreasing simultaneously NOx and soot emissions down to ultra-low levels, but real application in production engines of the massive EGR strategy is compromised by the ISFC-BSFC problem, while the Miller cycle strategy still needs further development to reduce BSFC.

7. Acknowledgments

The authors of this paper thank the Spanish Ministry of Economic and Competitively for the financial support of this research through the project TRA 2010-20271 (LOWTECOM).

References

1. Torres García M., Jiménez-Espadafor Aguilar F.J., and Sánchez Lencero T. "Experimental study of the performances of a modified diesel engine operating in homogeneous charge compression ignition (HCCI) combustion mode versus the original diesel combustion mode". Energy, Volume 34, Issue 2, pages 159–171, 2009.
2. Torregrosa A.J., Broatch A., Novella R. and Mónico L.F. "Suitability analysis of advanced diesel combustion concepts for emissions and noise control". Fuel, vol. 36, pages 825-838, 2011.
3. Benajes J., López J.J., Novella R, García A. "Advanced Methodology for Improving Testing Efficiency in a Single-Cylinder Research Diesel Engine". Exp Techniques 2008; 32:41-47.
4. Dec J.E. "Diesel-Fueled HCCI Engines," in Homogeneous Charge Compression Ignition (HCCI) Engines: Key Research and Development Issues Zhao, F. (Ed), SAE, Warrendale, PA, 2003.
5. ShiL., Cui Y., Deng K., Peng H. and Chen Y. "Study of low emission homogeneous charge compression ignition (HCCI) engine using combined internal and external exhaust gas recirculation (EGR)". Energy, Volume 31, Pages 2665-2676, 2006.
6. Saxena S., Bedoya I.D. "Fundamental phenomena affecting low temperature combustion and HCCI engines, high load limits and strategies for extending these limits". Progress in Energy and Combustion Science, vol. 39, 457-488, 2013.
7. Plee J.T., Myers J.P., and Ahmad T. "Flame Temperature Correlation for the Effects of Exhaust Gas Recirculation on Diesel Particulate and NOx Emissions," SAE 811195, 1981.
8. Ahmad T., and Plee S.L., "Application of Flame Temperature Correlations to Emissions from a Direct-Injection Diesel Engine," SAE 831734, 1983.
9. Dec J.E., and Canaan R.E., "PLIF Imaging of NO Formation in a DI Diesel Engine," SAE 980147, 1998.
10. Dec J. E., "A Conceptual Model of DI Diesel Combustion Based on Laser-Sheet Imaging," SAE Paper 970873, 1997.
11. Siebers D.L., and Higgins, B., "Flame Lift-off on Direct-Injection Diesel Sprays under Quiescent Conditions," SAE Paper 2001-01-0530, 2001.
12. Pickett L.M. and Siebers D.L., "Soot in Diesel Fuel Jets: Effects of Ambient Temperature, Ambient Density, and Injection Pressure," Combustion & Flame, Volume 138, Issues 1-2, 114-135, 2004.
13. Pickett L.M., Siebers D.L., "Soot Formation Near the Lift-Off Length". Int. J. Engine Research, vol.7, no.2, 103-130, 2006.
14. Pickett L.M. and Siebers D.L., "Non-sooting, low flame temperature mixing-controlled DI Diesel combustion," SAE Paper 2004-01-1399, 2004.
15. Benajes J., Molina S., Novella R. and Amorim R. "Study on low temperature combustion for light-duty Diesel engines". Energy and fuels, vol. 24, 355-364, 2010.
16. Maiboom A., Tauzia X. and Hétet J.F. "Experimental study of various effects of exhaust gas recirculation (EGR) on combustion and emissions of an automotive direct injection diesel engine". Energy, Volume 33, Pages 22-34, 2008.
17. Benajes J., Molina S., Martín J. and Novella R. "Effect of advancing the closing angle of the intake valves on diffusion-controlled combustion in a HD diesel engine". Applied Thermal Engineering, vol. 29, 1947-1954, 2009.
18. Jia M., Xie M., Wang T. and Peng Z. "The effect of injection timing and intake valve close timing on performance and emissions of diesel PCCI engine with a full engine cycle CFD simulation". Applied Energy, Volume 88, Issue 9, Pages 2967–2975, September 2011.
19. Benajes J., Novella R., García A. and Arthozoul S. "The role of in-cylinder gas density and oxygen concentration on late spray mixing and soot oxidation processes". Energy, vol. 36, 1599-1611, 2011.

20. Benajes J., Serrano J.R., Dolz V. and Novella R. "Analysis of an extremely fast valve opening camless system to improve transient performance in a turbocharged high speed direct injection diesel engine". International Journal of Vehicle Design, vol. 49, 192-213, 2009.
21. Hountalas D.T., Mavropoulos G.C. and Binder K.B. "Effect of exhaust gas recirculation (EGR) temperature for various EGR rates on heavy duty DI diesel engine performance and emissions." Energy. Vol. 33, 272-283, 2008.
22. Christian R., Knopf F., Jasmek A., Schindler W.A. New Method for the Filter Smoke Number Measurement with Improved Sensitivity. MTZ 1993; 54:16-22.
23. Bosch W. "The Fuel Rate Indicator: A New Measuring Instrument For Display of the Characteristics of Individual Injection". SAE Paper 1966; 660749.
24. Lapuerta M., Armas O., Hernández J.J. "Diagnostic of D.I. Diesel Combustion from In-Cylinder Pressure Signal by Estimation of Mean Thermodynamic Properties of the Gas". Applied Thermal Engineering, vol. 19, 513–529, 1999.
25. Payri F., Molina S., Martín J., Armas O. "Influence of measurement errors and estimated parameters on combustion diagnosis". Applied Thermal Engineering, vol. 26, 226–236, 2006.
26. Desantes J.M., Torregrosa A.J., Broatch A. and Olmeda P. "Experiments on the influence of intake conditions on local instantaneous heat flux in reciprocating internal combustion engines". Energy. Vol. 36, 60-69, 2011.
27. Star-CD Methodology, Version 3.26, CD-Adapco, 2005.
28. Dukowicz J.K. "A Particle-Fluid Numerical Model for Liquid Sprays", Comp. Physics, vol. 35, 229–253, 1980.
29. Huh K.Y. and Gosman A.D. "A phenomenological model of Diesel spray atomization" Proc. Int. Conf. On Multiphase Flows; 1991.
30. Reitz R.D. and Diwakar R. "Structure of high-pressure fuel spray" SAE Paper 870598, 1987.
31. Habchi C., Lafossas F.A., Beard P. and Broseta D. "Formulation of a One-Component Fuel Lumping Model to Assess the Effects of Fuel Thermodynamic Properties on Internal Combustion Engine Mixture Preparation and Combustion"; SAE Paper 2004-01-1996, 2004.
32. Duclos J.M., Zellat M., Duranti S., Liang Y., Kralj C. and Schmidt G. "Towards a universal combustion model in StarCD for IC engines: from GDI to HCCI and application to DI diesel combustion optimization". 13th International Multidimensional Engine Modeling User's Group Meeting, lecture number 12, Detroit (USA), 2003.
33. Colin O. and Benkenida A. "The 3-zones extended coherent flame model (ECFM3Z) for computing premixed/diffusion combustion" Oil and Gas Science and Technology - Review IFP, vol 59 (6), 593–609, 2004.
34. Akihama K., Takatori Y., Inagaki K., Sasaki S. and Dean A.M. "Mechanism of the smokeless rich diesel combustion by reducing temperature", SAE Paper 2001-01-0655, 2001.

Nomenclature

aTDC	After Top Dead Centre
A/F	Air – Fuel ratio (mass)
BP	Intake Boost Pressure
BSFC	Brake Specific Fuel Consumption
CAD	Crank angle degree
CA50	Angle when 50% of the fuel is burnt
CO	Carbon monoxide
CO_2	Carbon dioxide
CR_{ef}	Effective compression ratio
EGR	Exhaust Gas Recirculation
EoI	End of Injection
EP	Exhaust Pressure
FSN	Filter Smoke Number
HC	Unburned Hydrocarbon
HD	Heavy Duty
HSDI	High speed direct injection
ICO	Fuel indicated carbon monoxide
IDUR	Intake event duration
IHC	Fuel indicated unburned hydrocarbon
INOx	Fuel indicated nitrogen oxides
IP	Injection Pressure
ISFC	Indicated specific fuel consumption
Isoot	Fuel indicated soot
IVC	Intake Valve Closing (angle)
LTC	Low Temperature Combustion
MBF	Mass burnt fraction
MC-LTC	Mixing-Controlled low temperature combustion
NOx	Nitrogen Oxides
O_2	Oxygen
p	Pressure
RoHR	Rate of Heat Release
SoI	Start of Injection
T	Temperature
T_{ad}	Adiabatic flame temperature
T_{int}	Intake temperature
TDC	Top Dead Centre
V	Volume
VVA	Variable Valve Actuation
YO_2	Oxygen concentration in the cylinder
$YO_{2,SOC}$	Oxygen concentration in the cylinder at the start of combustion
$YO_{2,EOC}$	Oxygen concentration in the cylinder at the end of combustion
3D-CFD	Tri-dimensional Computational Fluid Dynamics
ϕ	Equivalence ratio

List of Figures

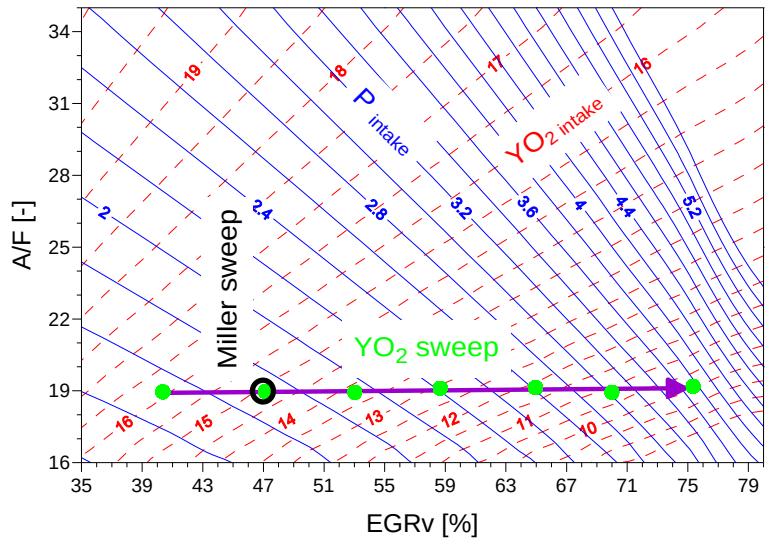

Figure 1: Engine map which summarizes most settings of the YO_2 sweep in round dots, remarked by an arrow. In this map, the Miller sweep appears as only one point, the empty black circle. Dashed lines are intake volumetric oxygen concentration and continuous lines represent the intake pressure.

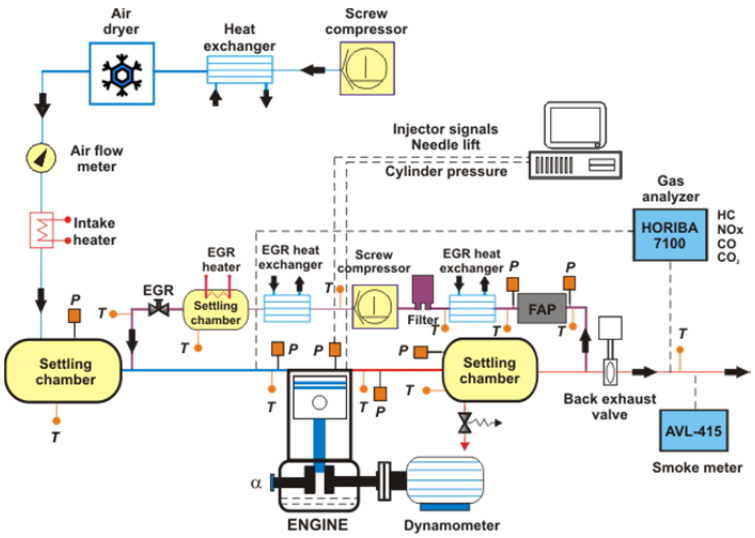

Figure 2: Complete test cell scheme.

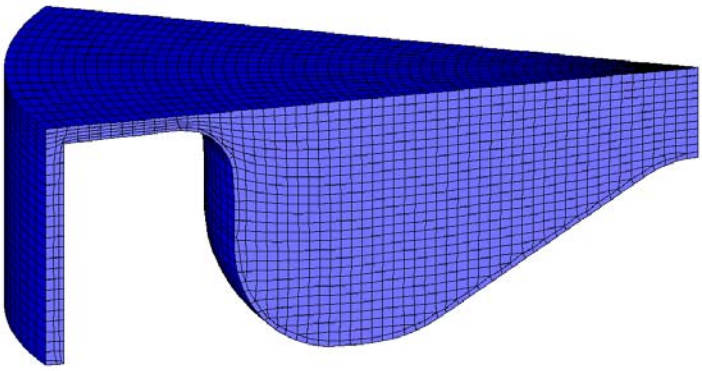

Figure 3: Computational grid at top dead centre.

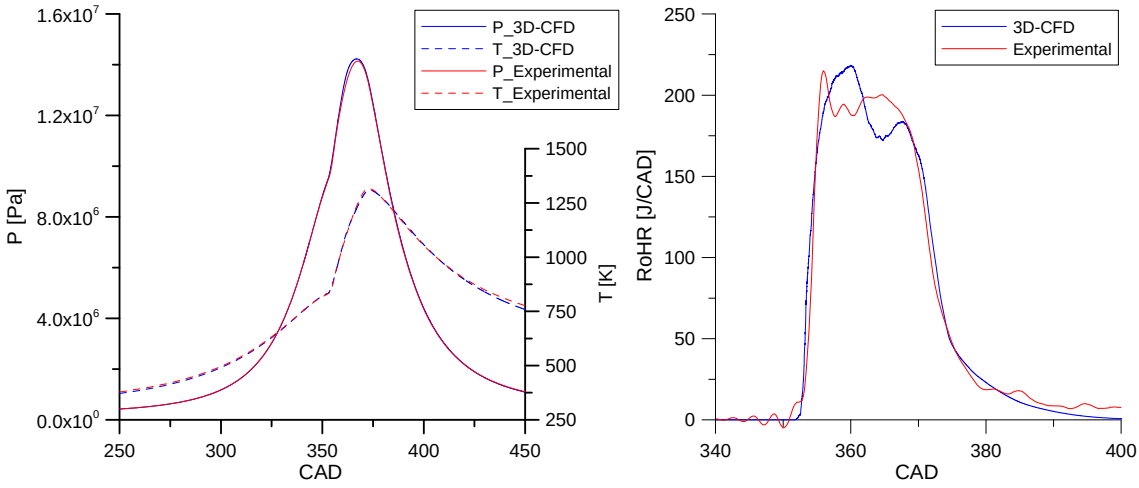

Figure 4: Computational model validation with experimental data.

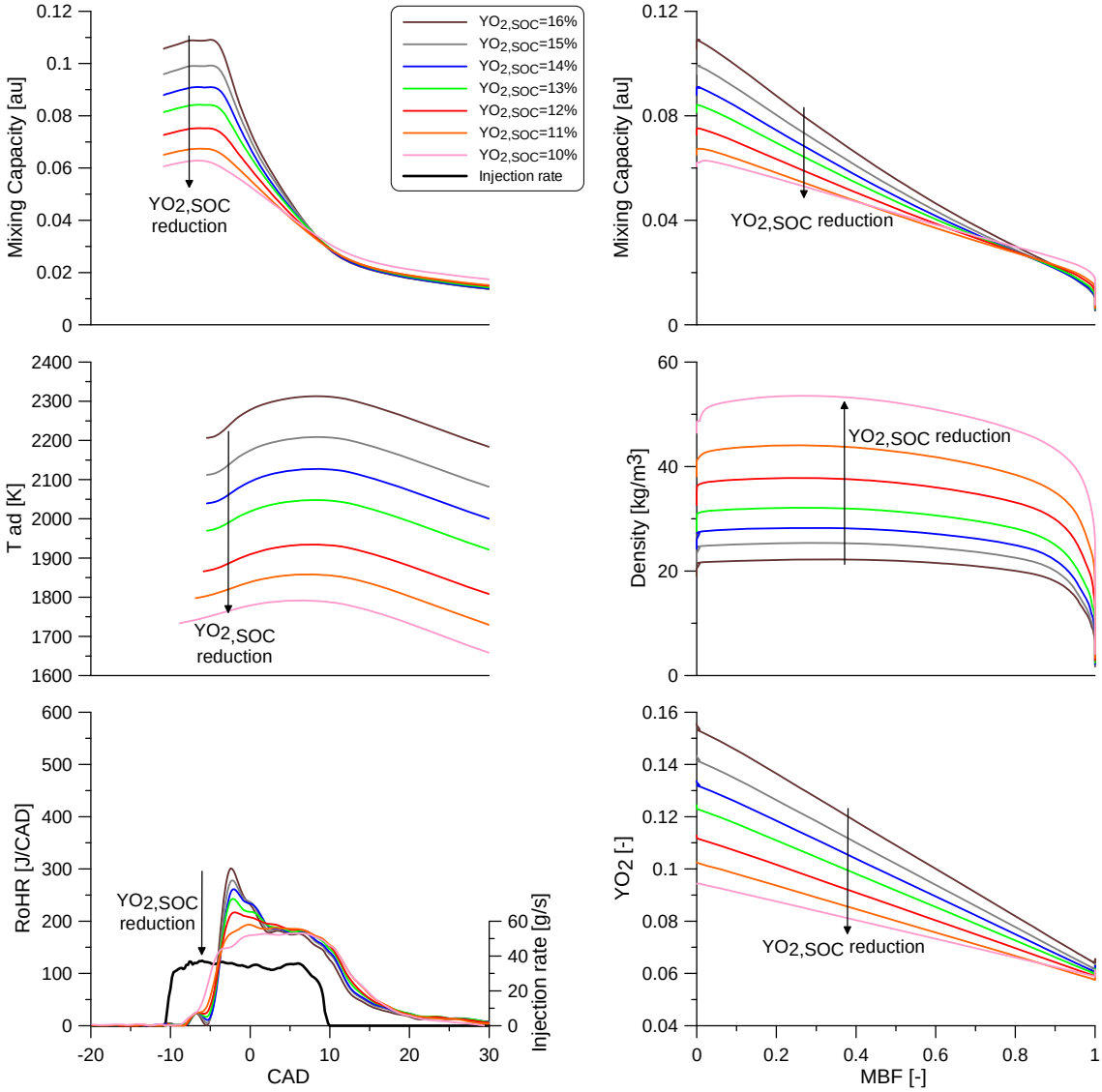

Figure 5: Results derived from experimental measurements. On the left, RoHR, adiabatic flame temperature and gas mixing capacity evolution from the $YO_{2,SOC}$ sweep. On the right, YO_2, density and gas mixing capacity as a function of the burned mass fraction.

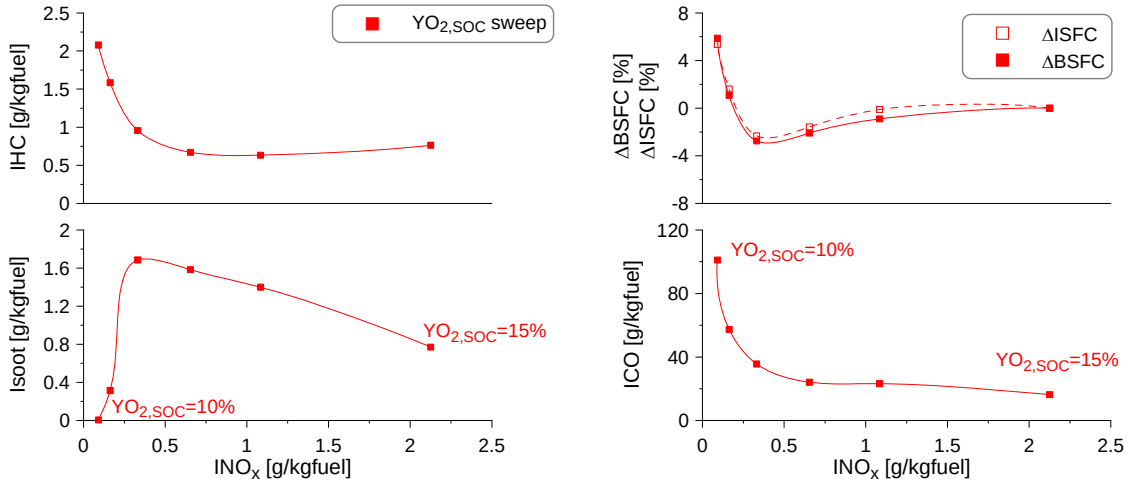

Figure 6: Measured fuel indicated engine-out emissions and fuel consumption evolution with the $YO_{2,SOC}$ sweep.

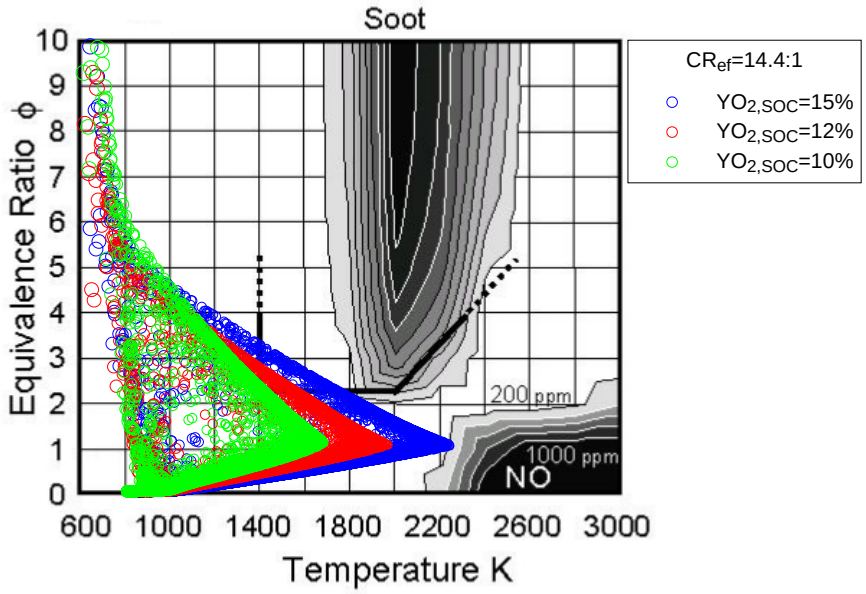

Figure 7: Model-predicted ϕ-T distribution. Comparison at CA50 for three levels of $YO_{2,SOC}$

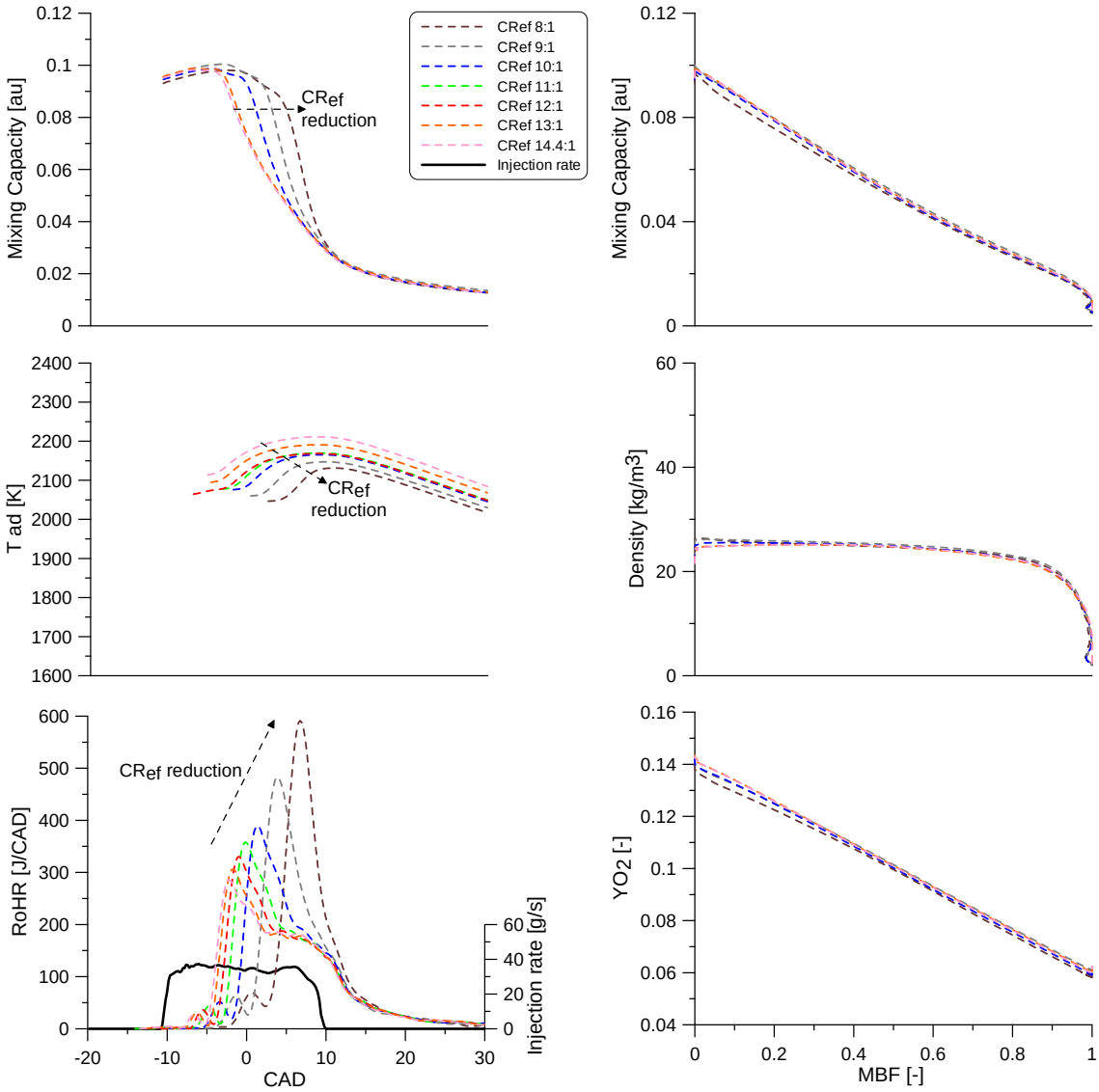

Figure 8: Results derived from experimental measurements. On the left, RoHR, adiabatic flame temperature and gas mixing capacity evolution from the CR_{ef} sweep. On the right, YO_2, density and gas mixing capacity as a function of the burned mass fraction.

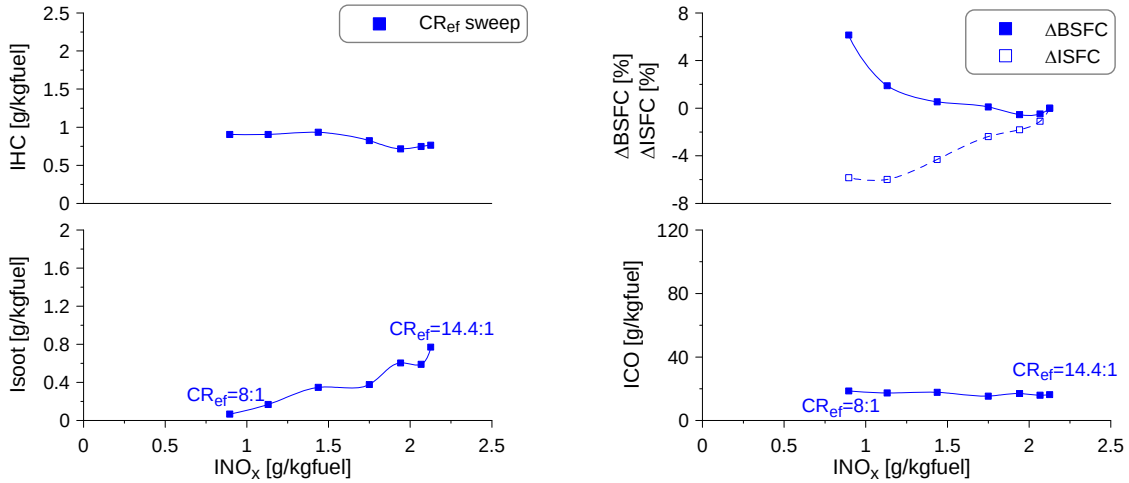

Figure 9: Measured fuel indicated engine-out emissions and fuel consumption evolution with the CR_{ef} sweep.

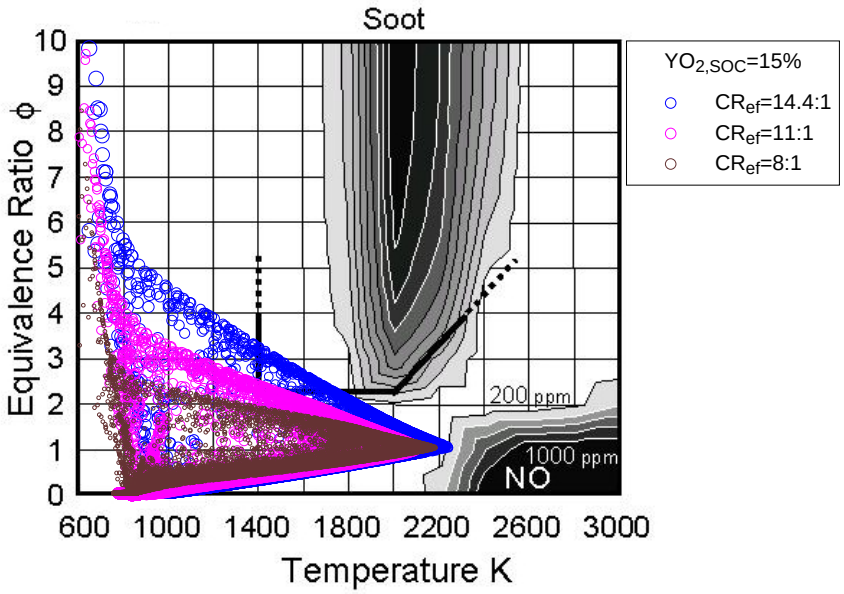

Figure 10: Model-predicted ϕ-T distribution. Comparison at CA50 for three levels of $CR_{ef.}$

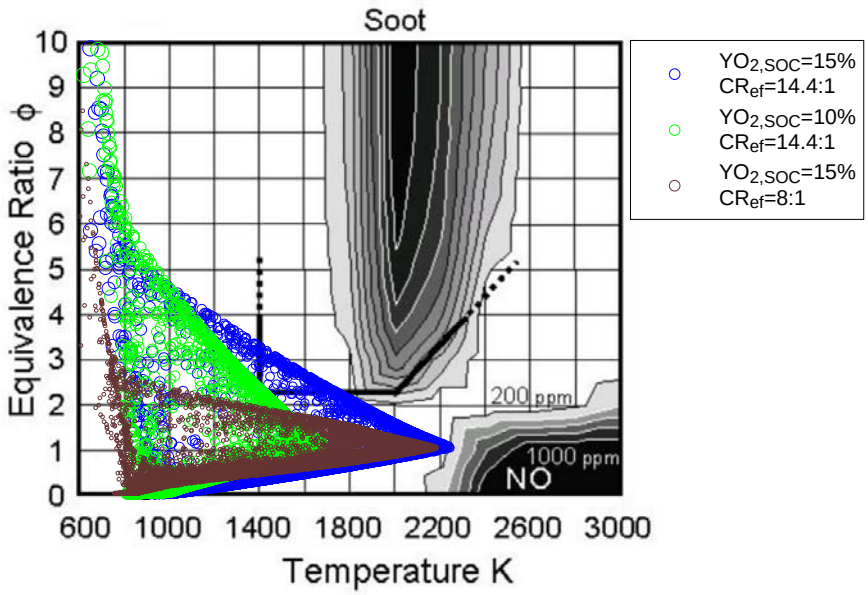

Figure 11: Model-predicted ϕ-T distribution. Comparison at CA50 for two levels of $YO_{2,SOC}$ and two different $CR_{ef.}$

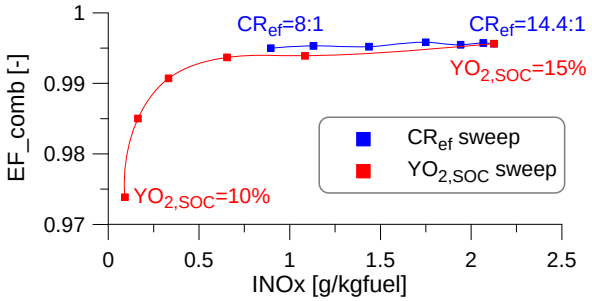

Figure 12: Combustion efficiency comparison between the $YO_{2,SOC}$ and the CR_{ef} sweeps. Results derived from experimental measurements.

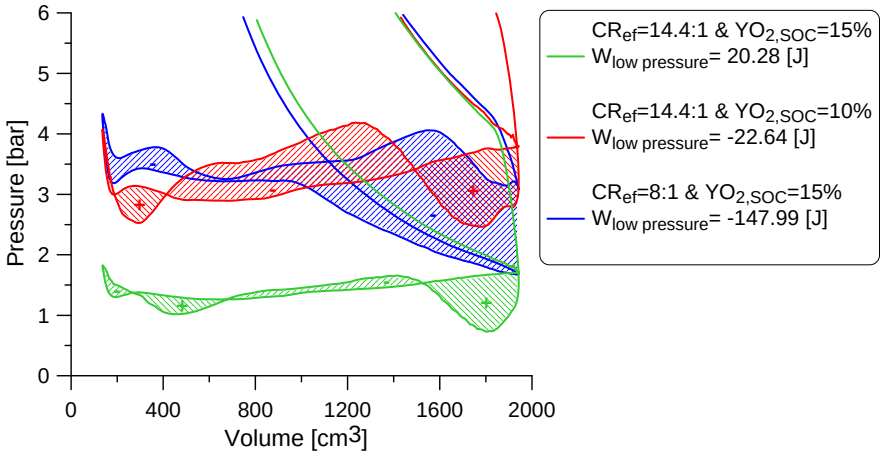

Figure 13: Measured low pressure loop from the p-V diagram, for two levels of $YO_{2,SOC}$ and two different $CR_{ef.}$

List of Tables

Table 1: Settings for testing the massive EGR strategy

Speed [rpm]	Load [%]	Fuel [mg/cycle]	IP [bar]	SoI [CAD aTDC]	T_{int} [degC]	CR_{ef} [-]	IDUR [CAD]	BP [bar]	EP [bar]	A/F [-]	$YO_{2,SOC}$ [%]	EGR [%]
1200	35	91.2	2350	-12	40	14.4:1	160	1.49	1.29	19	16	40.3
								1.65	1.45		15	47
								1.85	1.65		14	53
								2.1	1.9		13	58.7
								2.43	2.23		12	65
								2.89	2.69		11	71.4
								3.56	3.36		10	76.6

Table 2: Settings for testing the Miller strategy.

Speed [rpm]	Load [%]	Fuel [mg/cycle]	IP [bar]	SoI [CAD aTDC]	T_{int} [degC]	CR_{ef} [-]	IDUR [CAD]	BP [bar]	EP [bar]	A/F [-]	$YO_{2,SOC}$ [%]	EGR [%]
1200	35	91.2	2350	-12	40	14.4:1	160	1.65	1.45	19	15	47
						13:1	123	1.82	1.62			
						12:1	108	2.1	1.9			
						11:1	97	2.34	2.14			
						10:1	87	2.66	2.46			
						9:1	77	3.14	2.94			
						8:1	68	3.65	3.45			

Table 3: Engine basic specifications

Engine type	Single-cylinder, 4 stroke-cycle, direct injection, compression ignition
Bore x Stroke [mm]	123 x 152
Displacement [dm^3]	1.806
Compression ratio (nominal) [-]	14.4:1
Fuel injection system	Common-rail, Amplifier-piston
Injection nozzle	8 holes, 0.100 mm
Spray included angle [degrees]	140

Table 4: Accuracy of the instrumentation used in this work.

Variable measured	Device	Manufacturer and model	Accuracy
In-cylinder pressure	Piezoelectric transducer	Kistler 6125B	± 1.25 bar
Intake / exhaust pressure	Piezorresistive transducers	Kistler 4045A 10	± 25 mbar
Temperature in settling chambers and manifolds	Thermocouple	TC direct K type	± 2.5 degC
Crank angle, engine speed	Encoder	AVL 364	± 0.02 CAD
NOx, CO, HC, O_2, CO_2	Gas analyzer	HORIBA Mexa 7100 DEGR	4 %
FSN	Smoke meter	AVL 415	± 0.025 FSN
Gasoline / diesel fuel mass flow	Fuel balances	AVL 733S	± 0.2 %
Air mass flow	Air flow meter	Elster RVG G100	± 0.1 %